Using Spontaneous Emission of a Qubit as a Resource for Feedback Control

P. Campagne-Ibarcq,[1,2] S. Jezouin,[1,2] N. Cottet,[1,2] P. Six,[3,2] L. Bretheau,[1,2] F. Mallet,[1,2] A. Sarlette,[2] P. Rouchon,[3,2] and B. Huard[1,2,*]

[1]*Laboratoire Pierre Aigrain, Ecole Normale Supérieure-PSL Research University, CNRS, Université Pierre et Marie Curie-Sorbonne Universités, Université Paris Diderot-Sorbonne Paris Cité, 24 rue Lhomond, 75231 Paris Cedex 05, France*

[2]*Quantic Team, INRIA Paris-Rocquencourt, Domaine de Voluceau, B.P. 105, 78153 Le Chesnay Cedex, France*

[3]*Centre Automatique et Systèmes, Mines ParisTech, PSL Research University, 60 Boulevard Saint-Michel, 75272 Paris Cedex 6, France*

(Received 22 February 2016; published 1 August 2016)

Persistent control of a transmon qubit is performed by a feedback protocol based on continuous heterodyne measurement of its fluorescence. By driving the qubit and cavity with microwave signals whose amplitudes depend linearly on the instantaneous values of the quadratures of the measured fluorescence field, we show that it is possible to stabilize permanently the qubit in any targeted state. Using a Josephson mixer as a phase-preserving amplifier, it was possible to reach a total measurement efficiency $\eta = 35\%$, leading to a maximum of 59% of excitation and 44% of coherence for the stabilized states. The experiment demonstrates multiple-input multiple-output analog Markovian feedback in the quantum regime.

DOI: 10.1103/PhysRevLett.117.060502

Decoherence is generally considered as the main limitation to quantum information processing. It can be understood as an exchange of energy and information with the uncontrolled degrees of freedom of the environment leading to vanishing quantum superpositions and relaxation to equilibrium. For a two-level system, a ubiquitous source of decoherence comes from spontaneous emission into the electromagnetic modes of the environment. By monitoring the fluorescence of the system, it is then possible to track down its evolution during relaxation [1–4]. Here, we describe an experiment that uses the heterodyne detection signal of the fluorescence in order to counteract decoherence and preserve an arbitrary predetermined state of a superconducting qubit. We thus generalize the feedback scheme of previous proposals [5,6], based on the monitoring of a single quadrature of the fluorescence field, to both quadratures so that any predetermined state can be stabilized. In contrast with previously realized feedback control schemes based on a dispersive quantum nondemolition measurement (QND) [7–13], this protocol does not require any extra decoherence or measurement channel in addition to the unavoidable one that is spontaneous emission. Preserving a given qubit state is achieved with finite fidelity by performing rotations around the three axes of the Bloch sphere using driving fields (actuators), whose amplitude depends on the measured quadratures of the fluorescence field (sensors). The experiment thus constitutes a realization, in the most fundamental system, of multiple-input, multiple-output control in the quantum regime [14]. This is a key step towards the quantum error correction of complex systems [15,16].

Feedback protocol.—The fidelity of the stabilization of a quantum state relies crucially on the collection and detection efficiency of the fluorescence field. To maximize collection efficiency, a transmon qubit with transition frequency $f_q = 6.27$ GHz is placed inside an off-resonant copper cavity at 30 mK [Fig. 1(a)]. It is designed to channel most spontaneously emitted photons, by the Purcell effect [17], through a single dominantly coupled microwave port ("out" in Fig. 1) that accounts for more than 90% of the total cavity decay rate. The resulting qubit decay rate is measured to be $\gamma_1 = (4.7\ \mu\text{s})^{-1}$. The detection efficiency of both quadratures V_I and V_Q of the fluorescence field at f_q is maximized by using a Josephson Parametric Converter (JPC) [18–20]. After amplification, the signal is subsequently processed by the analog controller of the feedback loop at room temperature. The two quadratures V_I and V_Q encode information about the qubit relaxation and allow monitoring in real time of its quantum trajectory [3,4]. When integrated over a time dt, they are expressed as

$$\begin{aligned} V_I dt &= \sqrt{\tfrac{\eta\gamma_1}{2}}\langle\sigma_x\rangle dt + dW_I, \\ V_Q dt &= \sqrt{\tfrac{\eta\gamma_1}{2}}\langle\sigma_y\rangle dt + dW_Q, \end{aligned} \tag{1}$$

where $dW_{I,Q}$ are independent Wiener processes with variance dt modeling zero-point fluctuations and $\sigma_{x,y,z}$ are the Pauli operators. The total measurement efficiency was measured to be $\eta = 35\%$ (see Ref. [21]).

The goal of the feedback scheme is to reach and stabilize an arbitrary predetermined qubit state $|\Psi_{\theta,\varphi}\rangle = \cos(\theta/2)|e\rangle + \sin(\theta/2)e^{i\varphi}|g\rangle$, where θ and φ parametrize the Bloch sphere. This can be realized by controlling the qubit with the Hamiltonian $H_c = \hbar[u(t)\sigma_x + v(t)\sigma_y + w(t)\sigma_z]$ that depends linearly on the measured $V_I(t)$ and $V_Q(t)$. Physically, it corresponds to driving the qubit with a

microwave signal whose quadratures are modulated as $u(t) = \bar{u} + \delta u(t)$ and $v(t) = \bar{v} + \delta v(t)$ and whose angular frequency detuning with the qubit is $w(t)$. The protocol requires three controllers that are schematized by boxes in Fig. 1 and whose relevance will become clear in the following sections. (i) The Rabi box consists in driving the qubit with its own fluorescence field that is both amplified by a gain G_R and phase shifted by α. (ii) The frequency modulation (FM) box modulates the qubit frequency so that w is equal to the quadrature $V_\beta = V_I \cos\beta + V_Q \sin\beta$ multiplied by a gain G_{FM}. (iii) The Drift box performs static precompensation by adding a constant drive $(\bar{u}, \bar{v})$ independently of $V_{I,Q}$. The parameters of these three controllers determine the stabilized state. We now consider the following set of parameters in order to stabilize $|\Psi_{\theta,\varphi}\rangle$:

$$\text{(i)}\ G_R = \sqrt{\frac{\gamma_1}{8\eta}}(1+\cos\theta), \qquad \alpha = \pi/2,$$
$$\text{(ii)}\ G_{\mathrm{FM}} = \sqrt{\frac{\gamma_1}{8\eta}}\sin\theta, \qquad \beta = \varphi - \pi/2,$$
$$\text{(iii)}\ -\frac{\bar{u}}{\sin\varphi} = \frac{\bar{v}}{\cos\varphi} = \frac{\gamma_1}{8\eta}(\cos\theta - \eta)\sin\theta. \qquad (2)$$

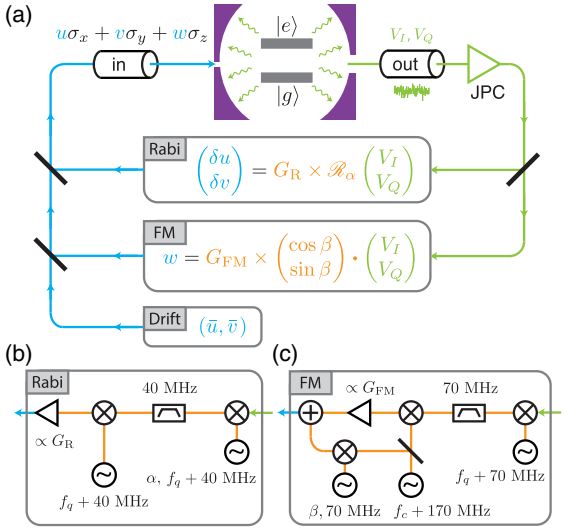

FIG. 1. Feedback scheme and its implementation. (a) An arbitrary state of a transmon qubit is stabilized by feedback control based on a continuous measurement of its fluorescence field quadratures $V_I(t)$ and $V_Q(t)$. The control Hamiltonian $H_c = \hbar[u(t)\sigma_x + v(t)\sigma_y + w(t)\sigma_z]$ depends linearly on $V_I(t)$ and $V_Q(t)$ and is designed to compensate in real time for the deviations of the qubit from its target state. The controller can be split into three physically distinct boxes. The Drift box adds a constant drive $(\bar{u}, \bar{v})$ for static precompensation. The Rabi box adds a drive term $(\delta u, \delta v)$ proportional to the fluorescence field quadratures rotated by an angle α. The FM box modulates the qubit frequency leading to a term w proportional to the quadrature $V_\beta = V_I \cos\beta + V_Q \sin\beta$ of the fluorescence field. (b),(c) Scheme of the physical realizations of the Rabi and FM boxes (see the text).

This choice is motivated by the ideal case of perfect efficiency ($\eta = 1$) and ideal conditions (negligible dephasing, propagation time, and infinite detection bandwidth B), where it would stabilize $|\Psi_{\theta,\varphi}\rangle$ exactly [21]. As expected, when all boxes are turned off, the qubit is stabilized in the ground state $|g\rangle = |\Psi_{\pi,0}\rangle$.

Stabilizing the excited state.—To start with, we aim at stabilizing the excited state $|\Psi_{0,0}\rangle = |e\rangle$ of the qubit. This target only involves the Rabi box of the feedback loop since, according to Eq. (2), $G_{\mathrm{FM}} = \bar{u} = \bar{v} = 0$ when $\theta = 0$. The fluorescence field is phase shifted by $\alpha = \pi/2$ before being sent back to the qubit. This can be qualitatively understood by noting that V_I (respectively, V_Q) gives information about qubit deviations from $|e\rangle$ in the x (y) direction of the Bloch sphere, which can be compensated for by applying rotations around the orthogonal y (x) direction.

To implement the Rabi box [Fig. 1(b)], the fluorescence field is first down-converted to 40 MHz and phase shifted by a mixer whose local oscillator has a tunable phase offset that is able to set α [21]. Then, this 40 MHz signal is filtered in the band 25–50 MHz in order to avoid heating the qubit with an important noise power, particularly at the transition frequency towards the higher energy levels of the transmon. Finally, the signal is up-converted back to f_q, and a series of amplifiers and variable attenuators allows one to control the overall gain G_R of the Rabi box.

By varying the parameters G_R and α, it is possible to maximize the excitation of the stabilized state (Fig. 2). The excitation is characterized by measuring the qubit after turning on the feedback protocol during a time 30 μs (much longer than γ_1^{-1}). Note that all shown tomographic measurements in this Letter are obtained by averaging the fluorescence signal (feedback off) over 5 μs with or without

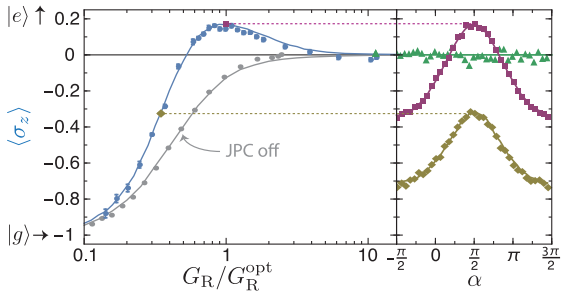

FIG. 2. Stabilization of the excited state. Targeting the excited state $|\Psi_{0,0}\rangle = |e\rangle$, the parameters G_{FM}, $\bar{u}$, and $\bar{v}$ are set to zero according to Eq. (2) (only the "Rabi box" of Fig. 1 is on). Measurements (symbols) and simulations (lines) represent $\langle\sigma_z\rangle$ as a function of gain G_R for fixed rotation angle $\alpha = \pi/2$ (left panel) and as a function of α for fixed $G_R/G_R^{\mathrm{opt}} = 0.35$, 1, 11.4 (right panel). The case where the JPC amplifier is turned on (off) is shown in blue (gray). The qubit is measured after a feedback sequence of 30 μs ensuring that it is in a steady state. Statistical uncertainties are indicated by error bars in the left panel and by symbol size in the right panel. All the parameters entering the simulations are measured independently.

an initial $\pi/2$ pulse on σ_x [21,22]. When setting $\alpha = \pi/2$, $\langle\sigma_z\rangle$ is measured as a function of the gain G_R and exhibits a maximum $\langle\sigma_z\rangle = 0.17$ at G_R^{opt} corresponding to an inverted population with 59% of excitation (blue in the left panel in Fig. 2). For the largest gains, the qubit reaches a maximal entropy state as evidenced by the measured $\langle\sigma_z\rangle = 0$ whatever α (green in the right panel in Fig. 2). There, control signals produce such large and noisy rotation angles that the qubit state is effectively randomized. Note that the coherences $\langle\sigma_x\rangle$ and $\langle\sigma_y\rangle$ were measured to be zero for all gain G_R. When the JPC is turned off ($\eta \simeq 0.005$, gray symbols), we observe that $\langle\sigma_z\rangle$ increases monotonically with G_R but saturates at 0. There, the detection efficiency is so small that the inputs of the Rabi box are just noisy signals with a negligible correlation with the qubit state. The qubit is then effectively heated by a thermal source, and population inversion never occurs.

The stationary state in the presence of feedback can be computed by solving numerically a stochastic master equation [14,21,23,24]. The relevant parameters, which are all measured independently, are the decay rate γ_1, measurement efficiency η, dephasing rate $\gamma_\phi = (22\ \mu\text{s})^{-1}$, finite bandwidth of the detection setup $B = 3.3$ MHz, and nonzero delay time $T_d \approx 0.12\ \mu$s. The data in both panels in Fig. 2 are in excellent agreement with simulations of the stochastic master equation (continuous lines). Further simulations show that the stabilized excitation is mainly limited to 59% because of the measurement inefficiency (see Table I in Ref. [21]). Note that in the experiment the gain G_R (respectively, phase α) is known up to some prefactor (respectively, offset). The simulations, which show that the maximum occurs at $G_R^{\text{opt}} = \sqrt{\gamma_1/2\eta}$ ($\alpha = \pi/2$), allow one to calibrate it.

Stabilizing a coherent superposition.—We now turn to stabilizing an arbitrary coherent state. In the work of Wang and Wiseman [6], it is shown that rotations around σ_x and σ_y alone (Rabi box) cannot stabilize states on the equator of the Bloch sphere. Therefore, we implement a feedback protocol that also uses rotations around the σ_z axis, which corresponds to modulating the qubit frequency [FM box in Fig. 1(c)]. It relies on the ac Stark shift effect: A drive close to cavity frequency $f_c = 7.86$ GHz induces an intensity-dependent shift of the qubit frequency [25,26]. For that purpose, the fluorescence signal is bandpass filtered (bandwidth $B_f = 2$ MHz $< B$) and up-converted to a frequency $f_c + \Delta$. We use a large enough detuning $\Delta = 100$ MHz so that the measurement-induced dephasing rate $\gamma_m = (84\ \mu\text{s})^{-1}$ remains much smaller than γ_1 for the parameters required by the feedback law [21]. In order to get w proportional to a single quadrature V_β, we combine the up-converted field, amplified by a gain G, with a large amplitude $\epsilon_0 e^{i2\pi(f_c+\Delta)t+i\beta}$ tone. Then, to first order,

$$w(t)/2\pi \propto |\epsilon_0 e^{i\beta} + G(V_I + iV_Q)|^2 \simeq \epsilon_0^2 + 2G\epsilon_0 V_\beta. \quad (3)$$

The gain $G_{\text{FM}} \propto G\epsilon_0$ of the FM box can thus be tuned by varying G [21]. In practice, the frequency offset due to ϵ_0^2 is equal to 810 kHz and simply renormalizes f_q throughout all the experiments.

To begin with, one can stabilize the state $|\Psi_{\pi/2,\pi/2}\rangle = (|e\rangle + i|g\rangle)/\sqrt{2}$ on the equator of the Bloch sphere. Therefore, according to Eq. (2), we set $\alpha = \pi/2$, $G_R = G_R^{\text{opt}}/2$, $\bar{u} = \gamma_1/8$, and $\bar{v} = 0$. The gain G_{FM} is then empirically set to the value $G_{\text{FM}}^{\text{opt}}$ that maximizes the coherences $\sqrt{\langle\sigma_x\rangle^2 + \langle\sigma_y\rangle^2}$. The optimal value for β can be found in Fig. 3(a), which shows the measured coherences $\langle\sigma_x\rangle$ and $\langle\sigma_y\rangle$ of the state stabilized by the feedback loop as a function of β. Simulations of the stochastic master equation are shown as continuous lines.

As can be seen, for $\beta = -10°$, the Bloch vector is in the direction of the target state with $\langle\sigma_x\rangle = 0$ and $\langle\sigma_y\rangle \approx 0.22$. The slight offset in β from 0 compared to Eq. (2) originates [21] from the neglected higher-order terms in Eq. (3). Now varying β, it can be seen [Fig. 3(a)] that $\langle\sigma_x\rangle$ and $\langle\sigma_y\rangle$ follow sinusoidal oscillations in quadrature. It indicates that any state on the equator of the Bloch sphere can be stabilized by just changing β, even though, here, the drifts $\bar{u}$ and $\bar{v}$ have not been adjusted to their optimal values for each value of β. We notice an overestimation of the

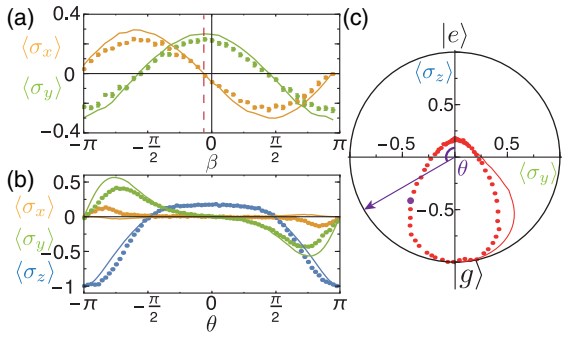

FIG. 3. Stabilization of any state. (a) Measured (symbols) and simulated (continuous lines) values of $\langle\sigma_x\rangle$ (orange) and $\langle\sigma_y\rangle$ (green) as a function of the phase β when targeting the state $|\Psi_{\pi/2,\pi/2}\rangle = (|e\rangle + i|g\rangle)/\sqrt{2}$. According to Eq. (2), one sets $G_R = G_R^{\text{opt}}/2$, $\alpha = \pi/2$, $\bar{u} = \gamma_1/8$, and $\bar{v} = 0$. The gain G_{FM} is experimentally set to its optimal value $G_{\text{FM}}^{\text{opt}}$ giving the maximum $\langle\sigma_x\rangle^2 + \langle\sigma_y\rangle^2$. The targeted state is most closely reached for $\beta = -10°$ (red) due to a slight nonlinearity in the FM box response [21]. As in Fig. 2, a comparison with the simulations serves as a calibration of the experimental offset on β. Statistical uncertainties are indicated by error bars (by symbol size in the other panels). (b) Measured (symbols) and simulated (continuous lines) values of $\langle\sigma_x\rangle$, $\langle\sigma_y\rangle$, and $\langle\sigma_z\rangle$ (respectively, orange, green, and blue) as a function of the polar angle θ of targeted state $|\Psi_{\theta,\pi/2}\rangle$. (c) Projection of the Bloch sphere on the yz plane. Red dots represent the measured stabilized states of (b). The corresponding simulated states are shown as a red line. A purple dot indicates the stabilized states when aiming for $\theta = 2\pi/3$.

amplitude of the coherences by the simulations. This mismatch between the experiment and simulation for $\theta > 0$ remains when considering various parasitic effects, such as the pollution of I and Q by the transmitted control fields through the cavity or the impact of internal cavity dynamics on measurement-induced dephasing and real-time qubit frequency modulation [21].

Since we have already shown how to tune the longitude of the stabilized state [Fig. 3(a)], we now fix $\beta = -10°$ and proceed to stabilize states $|\Psi_{\theta,\pi/2}\rangle$ of arbitrary polar angle θ. Measured stationary values of $\langle\sigma_x\rangle$, $\langle\sigma_y\rangle$, and $\langle\sigma_z\rangle$ are plotted in Fig. 3(b) as a function of θ and in the Bloch sphere representation in Fig. 3(c). The gain of the FM box is here set to $G_{\mathrm{FM}} = G_{\mathrm{FM}}^{\mathrm{opt}} \sin\theta$, and the other feedback parameters obey Eq. (2). As expected from feedback correcting for relaxation, the purity of the stabilized state is larger for targeted states closer to $|g\rangle$ (smaller values of $\langle\sigma_z\rangle$). The largest stabilized coherences reach 44%, and the feedback efficiency [8] is 0.43 on average. The latter are mainly limited by efficiency η and dephasing (see Table I in Ref. [21]). The mismatch between simulations and measurements is even stronger when targeting states with $\langle\sigma_z\rangle < 0$ and measured purities are significantly below expectation. The emergence of a nonzero $\langle\sigma_x\rangle$ close to the ground state in Fig. 3(b) can be explained by a constant detuning of the control fields $\bar{u}$ and $\bar{v}$ of a few kilohertz. Note that the feedback law Eq. (2) does not maximize the purity when $\eta < 1$. We propose an optimal scheme in the absence of dephasing and loop delay in Ref. [21].

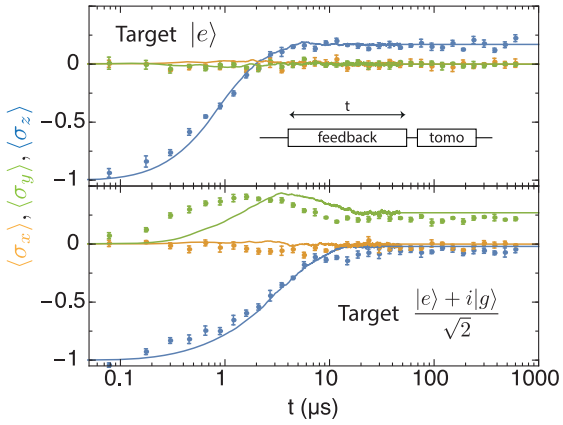

FIG. 4. Transient dynamics under feedback. Measured (symbols) and simulated (continuous lines) $\langle\sigma_x\rangle$, $\langle\sigma_y\rangle$, and $\langle\sigma_z\rangle$ (respectively, orange, green, and blue) as a function of the duration t of the feedback control. At $t = 0$, the qubit is in thermal equilibrium, and all control parameters in Fig. 1 are set to 0. The upper panel corresponds to the target state $|\Psi_{0,0}\rangle = |e\rangle$ [$G_R = G_R^{\mathrm{opt}}$, $\alpha = \pi/2$ as for the purple in Fig. 2(left)]. The lower panel corresponds to the target state $|\Psi_{\pi/2,\pi/2}\rangle = (|e\rangle + i|g\rangle)/\sqrt{2}$ [$\beta = -10°$ as for the red in Fig. 3(a)]. Error bars are statistical uncertainties. Simulations are performed with the same model as in Figs. 2 and 3(a).

Transient behavior.—In other continuous Markovian feedback schemes based on a dispersive measurement of a cavity [8] (respectively, on fluorescence [5,6]), the convergence rate towards the target state decreases towards zero as the target state approaches $|g\rangle$ or $|e\rangle$ (respectively, $|\Psi_{\pi/2,\varphi}\rangle$). In contrast, we show in Ref. [21] that, for any target on the Bloch sphere and any value of η, the qubit converges to the closest possible state at least at an exponential rate $1/T_1$. By varying the duration of the feedback protocol, it is possible to determine its dynamics when the qubit is initially in $|g\rangle$ (Fig. 4). When targeting the excited state, we observe, in excellent agreement with the simulations, that $\langle\sigma_z\rangle$ rises exponentially with a rate of about $4\gamma_1$. Once the stationary state is reached, it remains there permanently. When targeting the equator, $\langle\sigma_z\rangle$ still exhibits an exponential increase at a rate of about $1.5\gamma_1$ towards a stationary value, which is here just below zero due to imperfections of the feedback loop. In contrast, $\langle\sigma_y\rangle$ shows a bump at small times, showing that coherences initially increase for a few microseconds and then decrease. This behavior is qualitatively predicted by the simulations, although we do not obtain quantitative agreement when targeting the equator, possibly for the same reason as in Fig. 3(a).

Conclusion.—This set of experiments thus demonstrates that the information contained in both quadratures of the fluorescence of a qubit can be used to preserve an arbitrary predetermined state with finite fidelity using analog Markovian feedback. This technique is not exclusive but complementary to QND measurement-based feedback [7–13]. More generally, Markovian feedback can effectively modify the backaction associated to a measurement, which amounts to effectively engineering dissipation [27], in a similar manner to reservoir engineering schemes. The stabilization of manifolds in Hilbert spaces with more dimensions than two, which was recently demonstrated using autonomous feedback in qubit registers [28,29] or harmonic oscillators [30], may have counterparts using continuous measurement feedback [15,16] that could prove to be useful to quantum error correction. Our results could be applied to the wide variety of physical systems that decay by fluorescence.

We thank Michel Devoret, Emmanuel Flurin, Vladimir Manucharyan, Mazyar Mirrahimi, and the Quantronics group for fruitful discussions. Nanofabrication has been made within the consortium Salle Blanche Paris Centre. This work was supported by the EMERGENCES grant QUMOTEL of Ville de Paris and by the IDEX Program No. ANR-10-IDEX-0001-02 PSL*.

P. C.-I. and S. J. contributed equally to this work.

*benjamin.huard@ens.fr

[1] H. J. Carmichael, Quantum Trajectory Theory for Cascaded Open Systems, Phys. Rev. Lett. **70**, 2273 (1993).

[2] H. M. Wiseman and G. J. Milburn, *Quantum Measurement and Control* (Cambridge University Press, Cambridge, England, 2009).
[3] P. Campagne-Ibarcq, P. Six, L. Bretheau, A. Sarlette, M. Mirrahimi, P. Rouchon, and B. Huard, Observing Quantum State Diffusion by Heterodyne Detection of Fluorescence, Phys. Rev. X **6**, 011002 (2016).
[4] M. Naghiloo, N. Foroozani, D. Tan, A. Jadbabaie, and K. W. Murch, Mapping quantum state dynamics in spontaneous emission, Nat. Commun. **7**, 11527 (2016).
[5] H. F. Hofmann, G. Mahler, and O. Hess, Quantum control of atomic systems by homodyne detection and feedback, Phys. Rev. A **57**, 4877 (1998).
[6] J. Wang and H. M. Wiseman, Feedback-stabilization of an arbitrary pure state of a two-level atom, Phys. Rev. A **64**, 063810 (2001).
[7] C. Sayrin, I. Dotsenko, X. Zhou, B. Peaudecerf, T. Rybarczyk, S. Gleyzes, P. Rouchon, M. Mirrahimi, H. Amini, M. Brune, J.-M. Raimond, and S. Haroche, Real-time quantum feedback prepares and stabilizes photon number states, Nature (London) **477**, 73 (2011).
[8] R. Vijay, C. Macklin, D. H. Slichter, S. J. Weber, K. W. Murch, R. Naik, A. N. Korotkov, and I. Siddiqi, Stabilizing Rabi oscillations in a superconducting qubit using quantum feedback, Nature (London) **490**, 77 (2012).
[9] D. Ristè, C. C. Bultink, K. W. Lehnert, and L. DiCarlo, Feedback Control of a Solid-State Qubit Using High-Fidelity Projective Measurement, Phys. Rev. Lett. **109**, 240502 (2012).
[10] P. Campagne-Ibarcq, E. Flurin, N. Roch, D. Darson, P. Morfin, M. Mirrahimi, M. H. Devoret, F. Mallet, and B. Huard, Persistent Control of a Superconducting Qubit by Stroboscopic Measurement Feedback, Phys. Rev. X **3**, 021008 (2013).
[11] D. Ristè, M. Dukalski, C. A. Watson, G. de Lange, M. J. Tiggelman, Y. M. Blanter, K. W. Lehnert, R. N. Schouten, and L. DiCarlo, Deterministic entanglement of superconducting qubits by parity measurement and feedback, Nature (London) **502**, 350 (2013).
[12] P. Schindler, T. Monz, D. Nigg, J. T. Barreiro, E. A. Martinez, M. F. Brandl, M. Chwalla, M. Hennrich, and R. Blatt, Undoing a Quantum Measurement, Phys. Rev. Lett. **110**, 070403 (2013).
[13] G. de Lange, D. Ristè, M. J. Tiggelman, C. Eichler, L. Tornberg, G. Johansson, A. Wallraff, R. N. Schouten, and L. DiCarlo, Reversing Quantum Trajectories with Analog Feedback, Phys. Rev. Lett. **112**, 080501 (2014).
[14] A. Chia and H. M. Wiseman, Quantum theory of multiple-input-multiple-output Markovian feedback with diffusive measurements, Phys. Rev. A **84**, 012120 (2011).
[15] C. Ahn, H. M. Wiseman, and G. J. Milburn, Quantum error correction for continuously detected errors, Phys. Rev. A **67**, 052310 (2003).
[16] J. Wang, H. M. Wiseman, and G. J. Milburn, Dynamical creation of entanglement by homodyne-mediated feedback, Phys. Rev. A **71**, 042309 (2005).
[17] E. M. Purcell, Proceedings of the American Physical Society, spontaneous emission probabilities at radio frequencies, Phys. Rev. **96**, 681 (1946).
[18] N. Bergeal, F. Schackert, M. Metcalfe, R. Vijay, V. E. Manucharyan, L. Frunzio, D. E. Prober, R. J. Schoelkopf, S. M. Girvin, and M. H. Devoret, Phase-preserving amplification near the quantum limit with a Josephson ring modulator, Nature (London) **465**, 64 (2010).
[19] N. Roch, E. Flurin, F. Nguyen, P. Morfin, P. Campagne-Ibarcq, M. H. Devoret, and B. Huard, Widely Tunable, Nondegenerate Three-Wave Mixing Microwave Device Operating near the Quantum Limit, Phys. Rev. Lett. **108**, 147701 (2012).
[20] M. Hatridge, S. Shankar, M. Mirrahimi, F. Schackert, K. Geerlings, T. Brecht, K. M. Sliwa, B. Abdo, L. Frunzio, S. M. Girvin, R. J. Schoelkopf, and M. H. Devoret, Quantum back-action of an individual variable-strength measurement, Science **339**, 178 (2013).
[21] See Supplemental Material at http://link.aps.org/supplemental/10.1103/PhysRevLett.117.060502 for system characterization, details of the experimental setup, theoretical derivation of the closed-loop master equation, and simulation description and results.
[22] A. A. Houck, D. I. Schuster, J. M. Gambetta, J. A. Schreier, B. R. Johnson, J. M. Chow, L. Frunzio, J. Majer, M. H. Devoret, S. M. Girvin, and R. J. Schoelkopf, Generating single microwave photons in a circuit, Nature (London) **449**, 328 (2007).
[23] H. M. Wiseman and G. J. Milburn, Quantum Theory of Optical Feedback via Homodyne Detection, Phys. Rev. Lett. **70**, 548 (1993).
[24] H. M. Wiseman, Quantum theory of continuous feedback, Phys. Rev. A **49**, 2133 (1994).
[25] J. Gambetta, A. Blais, D. I. Schuster, A. Wallraff, L. Frunzio, J. Majer, M. H. Devoret, S. M. Girvin, and R. J. Schoelkopf, Qubit-photon interactions in a cavity: Measurement-induced dephasing and number splitting, Phys. Rev. A **74**, 042318 (2006).
[26] A. Blais, J. Gambetta, A. Wallraff, D. I. Schuster, S. M. Girvin, M. H. Devoret, and R. J. Schoelkopf, Quantum-information processing with circuit quantum electrodynamics, Phys. Rev. A **75**, 032329 (2007).
[27] S. G. Schirmer and X. Wang, Stabilizing open quantum systems by Markovian reservoir engineering, Phys. Rev. A **81**, 062306 (2010).
[28] S. Shankar, M. Hatridge, Z. Leghtas, K. Sliwa, A. Narla, U. Vool, S. M. Girvin, L. Frunzio, M. Mirrahimi, and M. H. Devoret, Autonomously stabilized entanglement between two superconducting quantum bits, Nature (London) **504**, 419 (2013).
[29] Y. Lin, J. Gaebler, F. Reiter, T. R. Tan, R. Bowler, A. Sørensen, D. Leibfried, and D. Wineland, Dissipative production of a maximally entangled steady state of two quantum bits, Nature (London) **504**, 415 (2013).
[30] Z. Leghtas *et al.*, Confining the state of light to a quantum manifold by engineered two-photon loss, Science **347**, 853 (2015).